Electron Cloud Spectroscopy Using Micro-Ring Fabry–Perot Sensor Embedded Gold Grating

A. E. Arumona, Anita Garhwal, Phichai Youplao, Iraj Sadegh Amiri, Kanad Ray, *Senior Member, IEEE*, S. Punthawanunt, and Preecha Yupapin

***Abstract*—An electron cloud spectroscopy system consisting of a microring and Bragg grating Fabry-Perot is proposed. It has the form of a Panda-ring formed by an add-drop filter with nonlinear two-phase modulators. The input light of 1.50μm center wavelength is fed into the system. By using suitable two-phase modulator parameters, the whispering gallery mode (WGM) of light is formed at the center ring. The gold plate at the center microring illuminated by light leads to electron cloud oscillations forming the electron density that results in the spin up and spin down of electrons. The electron cloud spins (spin up and spin down) form the qubits which can be transmitted to the Fabry-Perot sensing unit by the spin waves. The Fabry-Perot sensing unit measures the spectral profile of the electron cloud spins. To observe the spectral profile of the electron cloud spins a large bandwidth is employed. The space-time function is applied to distinguish the electron cloud spins, which leads to having the selected spin switching time and sensor sensitivity resolution. By varying the input power and the gold grating gaps, the change in optical path difference formed in terms of the electron cloud spins at the center ring, where the optimum of ~10Pbit is obtained. Both the reflection and transmission schemes of the microring Fabry-Perot circuit have bit rates of ~6Pbits^{-1}. The reflection and transmission spectra have a free spectral range of ~0.04-0.14μm. The optimum sensitivity of the microring Fabry-Perot sensor is 0.31μ m^{-1}.**

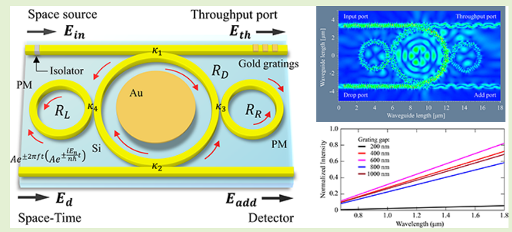

***Index Terms*— Fabry-Perot sensor, microring sensor, gold grating sensor.**

I. Introduction

Spectroscopy involves studying the behavior of light when it is emitted, absorbed, transmitted, or reflected by materials, which can be molecular or subatomic particles depending on the wavelength [1], [2]. The emitted, absorbed, transmitted, or reflected light by molecular or subatomic particles can be measured. The principle behind spectroscopy is the response of a material to light when the light illuminates such material. By plotting the response of the material as a function of the wavelength gives the spectrum. Many techniques and instruments are employed in spectroscopy [3]–[8]. Zvánovec *et al.* [10] used the Fabry-Perot interferometer to study the behavior of some selected gases. The Fabry-perot interferometer [11] can be used for sensing, telecommunication, and spectroscopy studies. The spectral resolution of the selected gases was obtained and compared with the results of other studies, which shows a good agreement. Yulianti *et al.* [12] designed a Fabry-Perot sensor, which was applied for humidity and temperature sensing. The reflection spectrum is in the range of 0-0.7. A narrow bandwidth has been employed for the sensing. The wavelength is in the range of 1549.6-1551.5nm. Pospori and Webb [13] had used the Fabry-Perot sensor for stress sensing study. The Fabry-Perot sensor consists of the Bragg gratings. The stress sensitivity exhibits linear relationship with the length of the Fabry-Perot cavity. The reflection spectrum is in the range of 0-1.0. A narrow bandwidth is employed for the study. The wavelength is in the range of 1.549-1.551μm. Wang *et al.* [14] designed a Fabry-Perot sensor for sensing application. The Fabry-Perot sensor consists of Bragg gratings. The study focused on the

Manuscript received April 20, 2020; revised May 10, 2020; accepted May 10, 2020. The associate editor coordinating the review of this article and approving it for publication was Dr. Carlos Marques. *(Corresponding author: Preecha Yupapin.)*

A. E. Arumona is with the Computational Optics Research Group, Advanced Institute of Materials Science, Ton Duc Thang University, Ho Chi Minh City 700000, Vietnam, also with the Faculty of Applied Sciences, Ton Duc Thang University, Ho Chi Minh City 700000, Vietnam, and also with the Division of Computational Physics, Institute for Computational Science, Ton Duc Thang University, Ho Chi Minh City 700000, Vietnam (e-mail: arumonaarumonaedward.st@student.tdtu.edu.vn).

Anita Garhwal and Kanad Ray are with the Amity School of Applied Sciences, Amity University Rajasthan, Jaipur 302002, India (e-mail: anitagarhwal@gmail.com; kanadray00@gmail.com).

Phichai Youplao is with the Department of Electrical Engineering, Faculty of Industry and Technology, Rajamangala University of Technology, Isan Sakon Nakhon Campus, Sakon Nakhon 47160, Thailand (e-mail: phichai.yo@rmuti.ac.th).

Iraj Sadegh Amiri and Preecha Yupapin are with the Computational Optics Research Group, Advanced Institute of Materials Science, Ton Duc Thang University, Ho Chi Minh City 700000, Vietnam, and also with the Faculty of Applied Sciences, Ton Duc Thang University, Ho Chi Minh City 700000, Vietnam (e-mail: irajsandegh@tdtu.edu.vn; preecha.yupapin@tdtu.edu.vn).

S. Punthawanunt is with the Faculty of Science and Technology, KasemBundit University, Bangkok 10250, Thailand (e-mail: suphanchai.pun@kbu.ac.th).

Digital Object Identifier 10.1109/JSEN.2020.2994240

measurement of temperature and concentration of liquid. The reflection spectrum is in the range of 0-1.0. A narrow bandwidth is employed for the study. The wavelength is in the range of 1548-1552nm. Tosi [15] applied the KLT method to study the sensing characteristics of the Fabry-Perot sensor. The KLT method is the Karhunen-Loeve transform method. The reflection spectrum is in the range of 0-90% (0-0.9). A narrow bandwidth is employed for the study. The wavelength is in the range of 1549-1551nm. Wada *et al.* [16] designed a Fabry-Perot sensor. The Fabry-Perot sensor consists of Bragg gratings and has the sensing ability to measure multi-point strain. The reflection spectrum of output signals is in the range of 0-3(arbitrary units). A narrow bandwidth is employed for the study. The wavelength is in the range of 1548.5-1552.0nm. Madan *et al.* [17] designed and fabricated a Fabry-Perot sensor for sensing application. The Fabry-Perot sensor is based on the Bragg gratings. The study focused on the measurement of strain and temperature. The reflection spectrum is in the range of 0-1.0. A narrow bandwidth is employed for the study. The wavelength is in the range of 1548.5-1552.0nm. The cost-effective Fabry-Perot interferometric micro-cavities are also interesting for applications [18]. In this work, the Fabry-Perot sensor is formed by Through port embedded gold grating. Change in optical path difference in a gold grating will be related to the electron oscillation on the sensing island. The microring Fabry-Perot structure is employed for the electron cloud generation, where the matching between the electron cloud optical path difference and the Fabry-Perot is the measurement. The circuit structure has the form of a Panda-ring [19], which has the advantage of the two-phase modulators, from which the whispering gallery mode (WGM) can be formed and used to trap the electrons and oscillate. Firstly, the Optiwave FDTD program will be applied to obtain the whispering gallery mode [20]. The used parameters will be extracted for the Matlab program. Secondly, the Matlab program is employed to simulate the spectral profile of the electron cloud spins where other results are obtained. The related theory is given, and simulation results are discussed.

II. Theoretical Background

The schematic and fabrication structure of the electron cloud spectroscopy is shown in Figure 1. The gold plate is embedded to form a sensor probe at the center microring coupled with a Bragg grating Fabry Perot sensing device. The interference of the Fabry Perot is coupled with the electron cloud generated by the silicon-gold layer given by [17]:

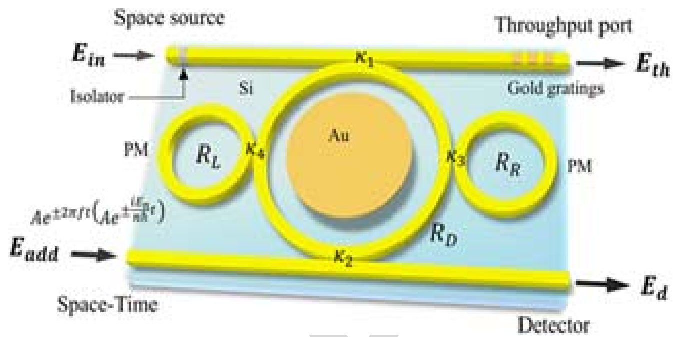

Fig. 1. A schematic diagram of a microring Fabry-Perot structure, where PM is the nonlinear phase modulator, the 1st space input source is the electric field. Gold plate is at the center ring with the Bragg gratings at the tips of the bus waveguide. The electrical fields of the input, throughput, add, and drop ports are E_{in}, E_{th}, E_{add} and E_d, respectively. $K_1 - K_4$: coupling constants. The isolator is applied to protect the feedback.

$$\boldsymbol{f\left(\Delta\phi\right) = 1 + cos\left(\Delta\phi\left(\lambda\right)\right)} \tag{1}$$

where $\Delta\phi\left(\lambda\right) = \boldsymbol{\frac{4\pi\eta_c g}{\lambda}},\Delta\phi$ is the phase difference, λ is the light source center wavelength, η_c is the refractive index of the waveguide, and g is defined as the gap between two Bragg gratings which are identical. The Bragg wavelength is $\lambda_B = 2n_{eff}\Lambda$, where n_{eff} is defined as effective refractive index, and Λ is defined as the grating period. The phase difference and the optical path difference relationship is given by OPD= $(\lambda/2\pi)$. $\Delta\phi$, where $\Delta\phi$ is the phase difference of the Fabry Perot interferometer.

The amplitude reflection coefficient is given in equation (2), shown at the bottom of this page, while the amplitude transmission coefficient is given in equation (3), shown at the bottom of this page,

where k, σ, and L_{AU} are the ac coupling coefficient, dc coupling coefficient and length of grating.

The reflection and transmission spectrums [14] are given in equations (4 and 5), respectively.

$$\boldsymbol{R = f\left(\Delta\phi\right)r} \tag{4}$$

$$\boldsymbol{T = \frac{1}{1 + Fsin^2\left(\phi - \frac{\phi}{2}\right)}} \tag{5}$$

where $F = \frac{4R_g}{\left(1-R_g\right)^2}$, $R_g = |r|^2$, $\phi = \frac{2\pi n_{eff}}{\lambda}.2e$, ϕ is the phase retardation.

$$\boldsymbol{r = \frac{-ksinh\left(\sqrt{\left(k^2g^2 - \sigma^2g^2\right)}\right)}{\sigma sinh\left(\sqrt{\left(k^2g^2 - \sigma^2g^2\right)}\right) + j\left(\sqrt{\left(k^2 - \sigma^2\right)}\right)cosh\left(\sqrt{\left(k^2g^2 - \sigma^2g^2\right)}\right)}} \tag{2}$$

$$\boldsymbol{t = \frac{1}{cosh\left(\sqrt{\left(k^2g^2 - \sigma^2g^2\right)}\right) - j\left(\frac{\sigma}{\sqrt{\left(k^2-\sigma^2\right)}}\right)sinh\left(\sqrt{\left(k^2g^2 - \sigma^2g^2\right)}\right)}} \tag{3}$$

The electric field is the input light given as [21]:

$$E_{in} = E_o \cdot \exp\left(-ik_z z\right) \tag{6}$$

where wavenumber is defined by $k_z = \frac{2\pi}{\lambda}$, and initial amplitude of the field is given by E_o, the propagation distance is defined by z, and λ is the input optical field wavelength.

The space-time function is applied for polariton spin-wave projection, which is given by

$$E_{add} = A\ e^{\pm i\omega t} \tag{7}$$

where t is defined as time, ω is defined as the angular velocity, and A is defined as the amplitude. The $\pm$ sign indicates both axis of time. The nonlinear effect known as the Kerr effect, is given as $\mathbf{n} = n_0 + n_2\ \mathbf{I} = n_0 + n_2 P / A_{eff}$, where n_0 and n_2 are the linear and nonlinear refractive indices respectively. I is the optical intensity, P is the optical power, A_{eff} is defined as the effective core area of the waveguide.

The coupling between light and electron in metal is described by the Drude model [22], which is given as:

$$\epsilon\left(\omega\right) = 1 - \frac{ne^2}{\epsilon_0 m\omega^2} \tag{8}$$

where ϵ_0 is defined as the relative permittivity. The electron density, charge and mass are defined as n, e, m respectively. ω is the angular frequency. At resonance, angular frequency becomes plasma frequency given as:

$$\omega_p = \left[\frac{ne^2}{\epsilon_0 m}\right]^{-1/2} \tag{9}$$

From equation (9) the electron density $n = \frac{\omega_p^2}{e^2}\epsilon_0 m$. The output fields of the structure are described as [23].

$$E_{th} = m_2 E_{in} + m_3 E_{add} \tag{10}$$

$$E_d = m_5 E_{add} + m_6 E_{in} \tag{11}$$

where the terms m_2, m_3, m_5, m_6 in equations (10 and 11) are defined in the given [24].

From equations (10 and 11), the normalized intensities of the system output are given by

$$\frac{I_{th}}{I_{in}} = \left[\frac{E_{th}}{E_{in}}\right]^2 \tag{12}$$

$$\frac{I_d}{I_{in}} = \left[\frac{E_d}{E_{in}}\right]^2 \tag{13}$$

III. Simulation Results

The microring Fabry-Perot structure in Figure 1 is simulated using the Optiwave FDTD program, which is 32-bit version 12.0 [25]. The grid size for the simulation has been implemented automatically by the program. The number of mesh cell are 209, 37, 269 for the three axes (x, y, z). The structure has one input port, two output ports (throughput and drop ports), and one port (add port) for modulation or multiplexing. The input light of 1.50μm is fed into the structure via the input port. The structure has a Panda-ring form, which enables to exhibit its nonlinearity effect. The waveguide material is silicon. The geometric parameters of the waveguide are given in Table I. The two small rings at the size of the center microring act as phase modulators, which can induce the nonlinearity effect that results in the trapping of light at the center microring to form the whispering gallery mode (WGM) as shown in Figure 2(a). The suitable parameters are as given in Table I. The electric field distribution of the trapped electron

TABLE I
THE SELECTED SIMULATION PARAMETERS [19], [26]

Parameters	Symbols	Values	Units
Input light power	P	100	mW
Gold plate radius	R_{Au}	0.2-2.8	µm
Gold plate thickness	T_{Au}	0.1-7.5	µm
Ring resonator radius	R_s	3.0	µm
Gold conductivity	σ	4.11×10^{7}	Sm^{-1}
Gold resistivity	ρ	2.44×10^{-8}	Ωm
Coupling coefficient	κ	0.06-0.70	
Insertion loss	γ	0.50	dB
Au refractive index	n	1.80	
Si refractive index	n_{Si}	3.42	
Si nonlinear refractive index	n_2	1.3×10^{-13}	m^2W^{-1}
Optical centre wavelength	λ	1.50	µm
Au grating gap	g	200-1000	nm
Au grating width	W_{AU}	1.3	µm
Au grating thickness	d	0.5	µm
Au grating length	L_{AU}	1.5	µm
Plasma frequency	ω_p	1.299×10^{16}	$rads^{-1}$
Core effective area	A_{eff}	0.30	μm^2
Free space permittivity	ϵ_o	8.85×10^{-12}	Fm^{-1}
Electron mass	m	9.11×10^{-31}	kg
Electron charge	e_o	1.60×10^{-19}	Coulomb
Waveguide loss	α	0.50	$dB.(mm)^{-1}$
Grating period	Λ	1.5-2.3	µm
Si-Waveguide length	L_{wg}	18.0	µm
Si-Waveguide width	W_{wg}	1.5	µm

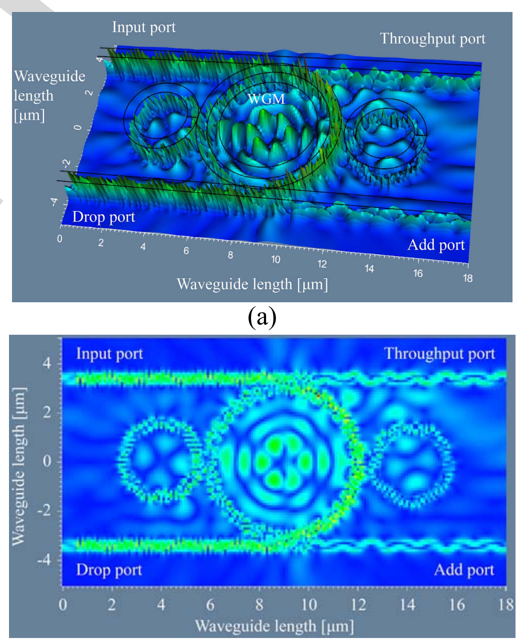

Fig. 2. Plot of the Optiwave FDTD results, where (a) the WGM formed at the center of the microring Fabry-Perot structure using suitable parameters in Table I, (b) the electric field distribution of the trapped electron cloud of the circuit.

cloud in the microring system is shown in Figure 2(b). The gold plate embedded at the center of the microring forms the polaritons and oscillation of plasmonic waves. The simulation results from the Optiwave FDTD program are extracted and used by the Matlab program. The interference signals of the structure are given in equation (1). The input light (electric field) as described in equation (6) is fed into the system (as described in equations (10 and 11)) via the input port and at the add port, the input light (space source) is multiplexed with time to form the space-time function as described in equation (7).

The input light excites the gold plate at the center of the microring leading to electron cloud oscillations that forms the electron density $[n = \frac{\omega_p^2}{e^2}\epsilon_0 m]$ which results in the spin-up $|\uparrow\rangle$ ($|o\rangle$) with the spin matrix $\frac{\hbar}{2}\begin{vmatrix} 0 & -i \\ i & 0 \end{vmatrix}$, and spin-down $|\rangle$ ($|\downarrow\rangle$) with the spin matrix $\frac{\hbar}{2}\begin{vmatrix} 0 & 1 \\ 1 & 0 \end{vmatrix}$. The electron density of trapped electron cloud can be transported via cable connection through the throughput and drop ports. The microring Fabry-Perot sensor has the Bragg grating. The amplitude reflection and transmission coefficients for the Fabry-Perot Bragg gratings are described in equations (2) and (3). Both the amplitude reflection and transmission coefficients are a function of the wavelength (λ). The reflection and transmission of the Fabry-Perot Bragg gratings have strong coupling interaction only in the range of the gap between two Bragg gratings which are identical. The resonance of the reflection and transmission sensing schemes is formed by the range of the optical path length of the two Bragg gratings.

The reflection and transmission spectra of the microring Fabry-Perot structure are described in equations (4) and (5), which are a function of the wavelength. The interference is a function of the phase difference $\Delta\phi(\lambda)$ of the Bragg gratings reflected light, which is related to the optical path difference of the electron cloud density. Figure 3 is the plot of the interference spectrum formed by the electron cloud and the normalized ED at the output described in equations (12) and (13). The interference spectra of the transmission and reflection with a varied Bragg grating gap of 200-1000nm are plotted, and the interference fringes are seen. The spin-wave components are the spin-up (blue colour) at the through-put port and the spin-down (red colour) at the drop port. Figure 4 is the plot of the normalized reflection spectrum. The reflection spectrum gives the measure of the reflected electron cloud as a function of OPD (wavelength) with a varied Bragg grating gap of 200-1000nm. Figure 5 is the plot of the normalized transmission spectrum with a varied Bragg grating gap of 200-1000nm. The transmission spectrum gives the measure of the transmitted electron cloud as a function of the wavelength. The plot of the sensor sensitivity is shown in Figure 6. The sensor sensitivity is $0.31(\mu m)^{-1}$, which is useful for electron cloud microscopic investigation in terms of optical path difference (OPD). In application, this system can be used for different sensing technology, where the gold plate presents the sensing probe, the Fabry-Perot acts as a spectroscopic sensor in terms of the optical path difference measurement.

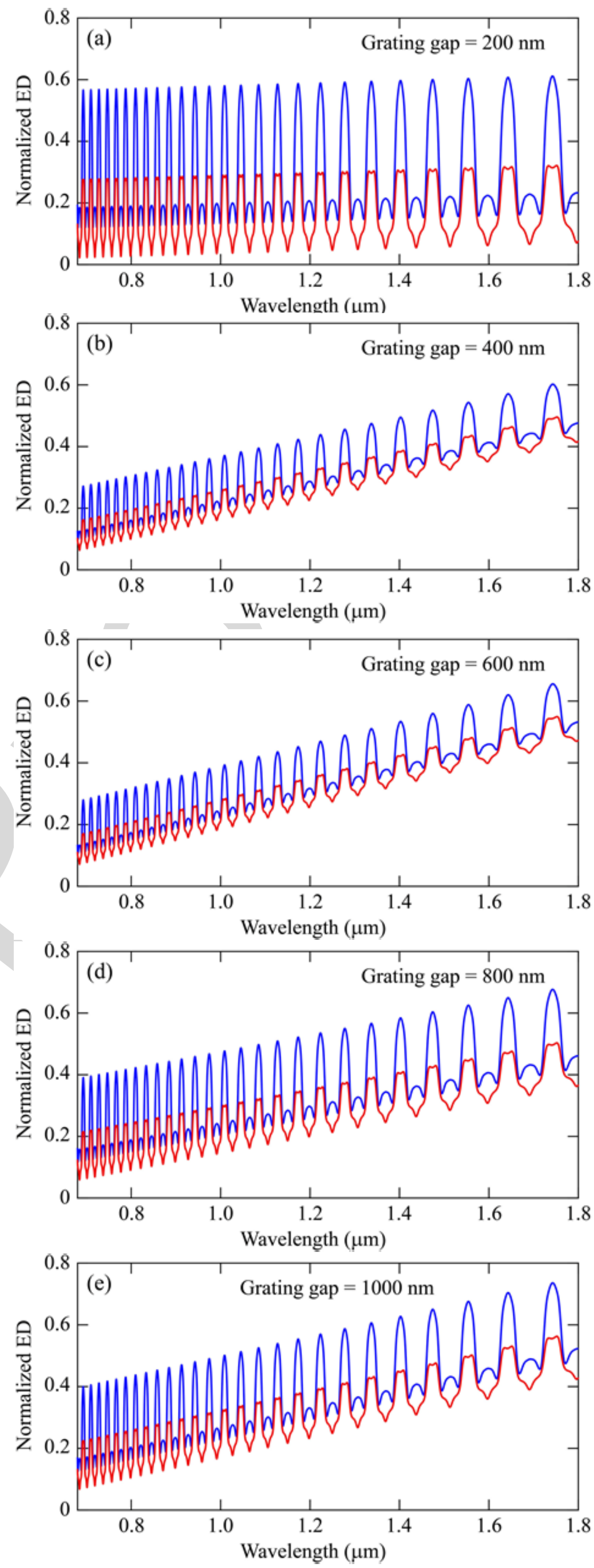

Fig. 3. The plot of the Fabry-Perot interference fringes. The Bragg grating gaps are varied from 200-1,000nm. The transmission fringes are plotted from (a)–(e), where the blue color is spin-up, and red color is spin-down of the transmitted spin-waves. The input power is fixed at 100 mW.

In this work, the Fabry-Perot sensor is used in the sensing and measurement related to the change in electron cloud spin waves (spin up and spin down), in which the change in optical path length of light within the gold grating causes

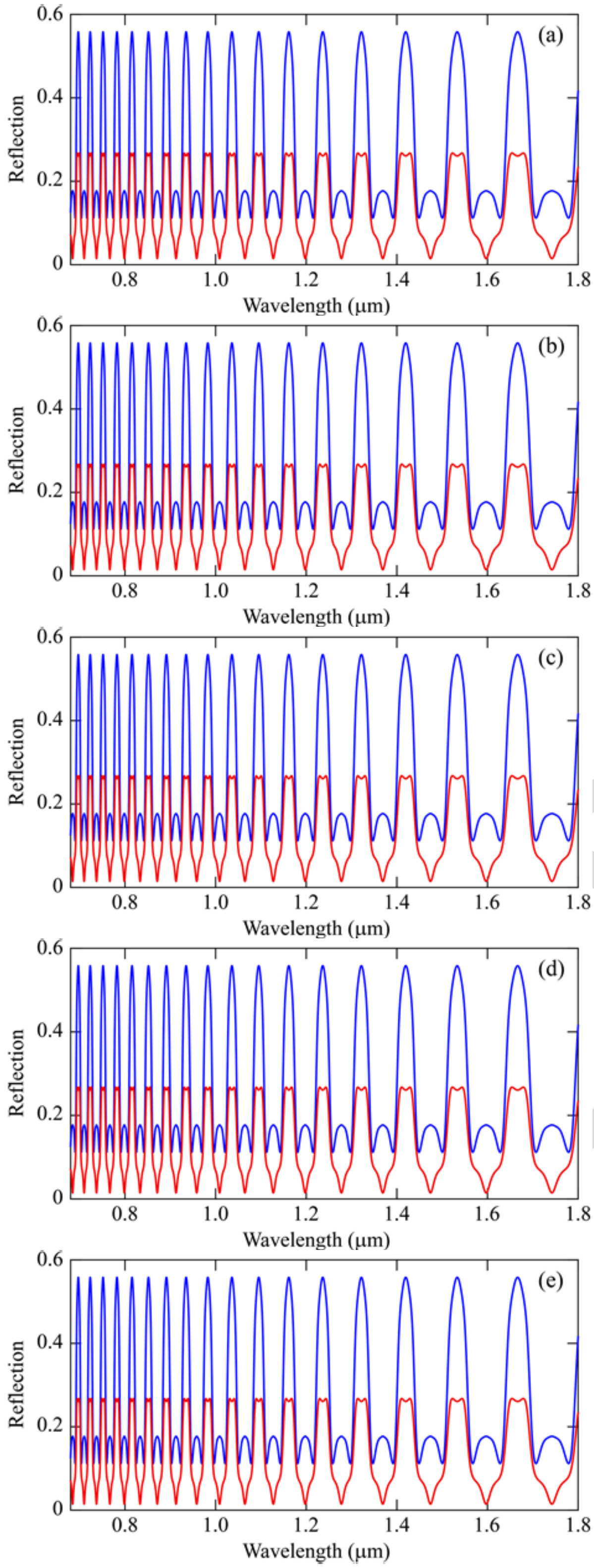

Fig. 4. Plot of the normalized reflection spectrum for 200-1000nm Bragg grating gaps, where the blue color is spin-up and red color is spin-down. The optimum free spectral range of the output signals is ∼0.14 μm. The changes in interference fringes are seen and used for Fabry-Perot sensors. The free spectral range (FSR) is the spacing between two successive qubits (spin-up and spin-down), which is 0.14μm for the optimum determined from the graph. The increase in the FSR gives a clearer picture or representation of the electron cloud spins.

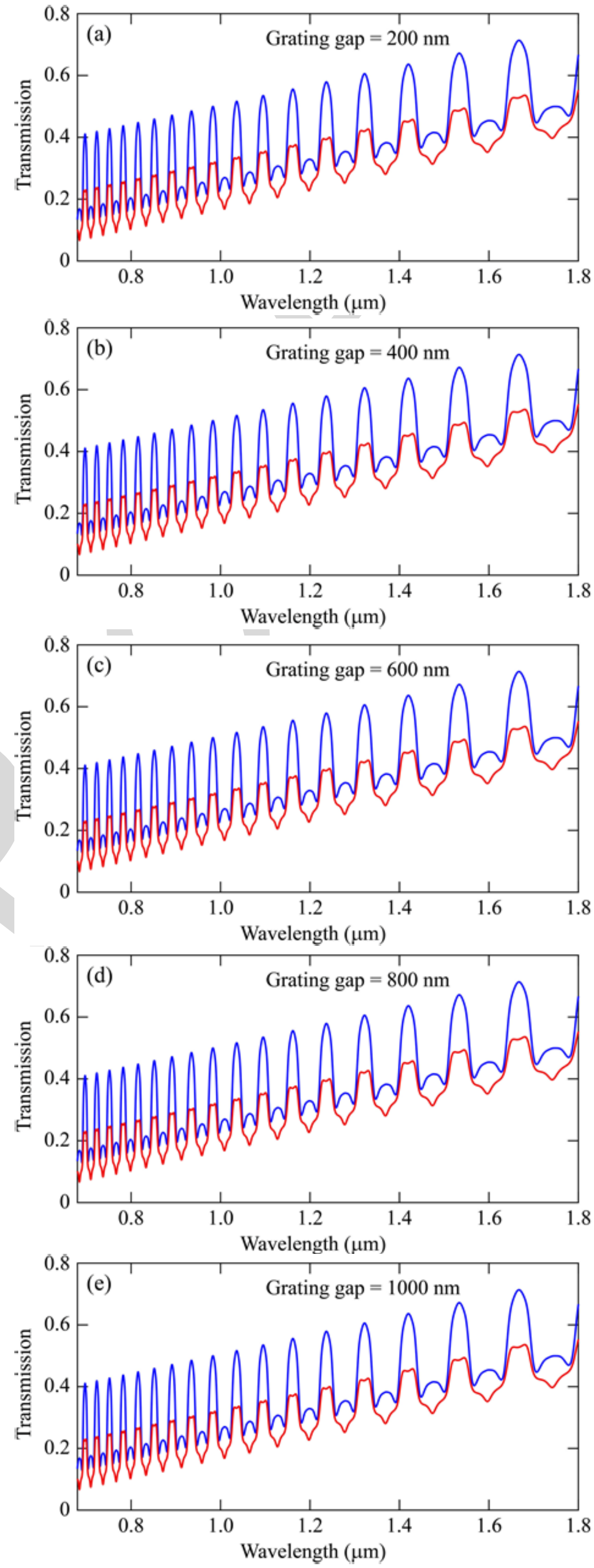

Fig. 5. Plot of the normalized transmission spectrum for 200-1000nm Bragg gratings gap where the blue color is spin-up and red color is spin-down. The optimum free spectral range of the output signals is ∼0.14 μm. The changes in interference fringes are seen and used for Fabry-Perot sensors.

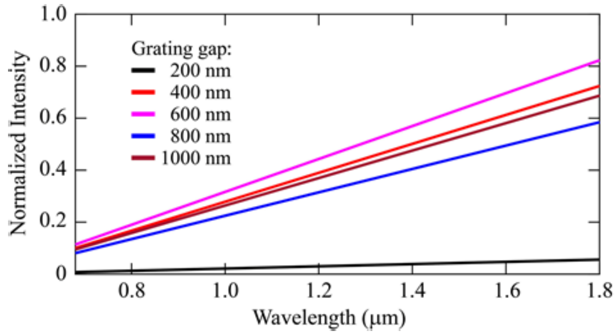

Fig. 6. Plot of the relationship between the input power and wavelength shifted. The sensor sensitivity is 0.31μm^{-1}, which is useful for electron cloud microscopic investigation in terms of optical path difference (OPD) in the Fabry-Perot sensors. The grating gaps are varied from 200-1000nm. The normalized intensity is equal to the power transferred per unit area.

the change in the electron cloud density(spin number). The change in optical path length of light within the Fabry-Perot cavity (gold grating) can introduce the change in electron cloud density (spin number) at the center ring, which can be balanced by adjusting the OPD. The change in OPD is related to the electron spins, which becomes the measurement. The central wavelength is 1.50μm, while the bandwidth of the gold grating in the wavelength domain is from 0.8-1.8μm. By using the large bandwidth, the large spin number of the electron cloud can be obtained. The increase in the number of qubits (spin-up and spin-down) can be observed in terms of electron density (ED) at the reflected and transmitted output ports. Large bandwidth optical field is employed to obtain large number of trapped electrons (electron cloud) properly. Grating bandwidth can be increased by a short grating length with a long period is applied. The ac and dc coupling coefficients can be increased, as shown in equations (2) and (3). The grating period and specific parameters are given in Table I. There is no specific effect of the spin matrix on the Fabry-Perot interference fringes. The spin matrix is the representation of the electron cloud spins (spin up and spin down) in matrix form.

As shown in Figure 7(a)-(b), the free spectral range (FSR) of the reflection and transmission spectra are obtained directly from the graph, which is the spacing between two successive qubits (spin up and spin down). The optimum FSR is 0.14μm. As shown in Figure 7(c)-(e) the number of bits per second is obtained from the relation $\frac{No.\ of\ bits}{one\ second}$. From Figure 7(c)-(e), the number of bits in one femtosecond (10^{-15}s) is 10 bits. The number of bits per second is 10Pbits^{-1} for the interference spectrum, while for both the reflection and transmission spectrum is 6Pbits^{-1}. The electron cloud density is transmitted by the spin waves to the Fabry-Perot sensing unit. The space-time function distinguishes the electron cloud spins by the time sequence known as quantum cellular automata [27]. The electron cloud is transmitted by the spin-waves to the Fabry-Perot sensing arm and as a result, coupled with the interference of the Fabry-Perot. The phase difference $\Delta\phi$ of the Fabry-Perot interferometer and the optical path difference of light results the change in the electron cloud density. The phase difference $\Delta\phi$ of light in the Fabry-Perot interferometer

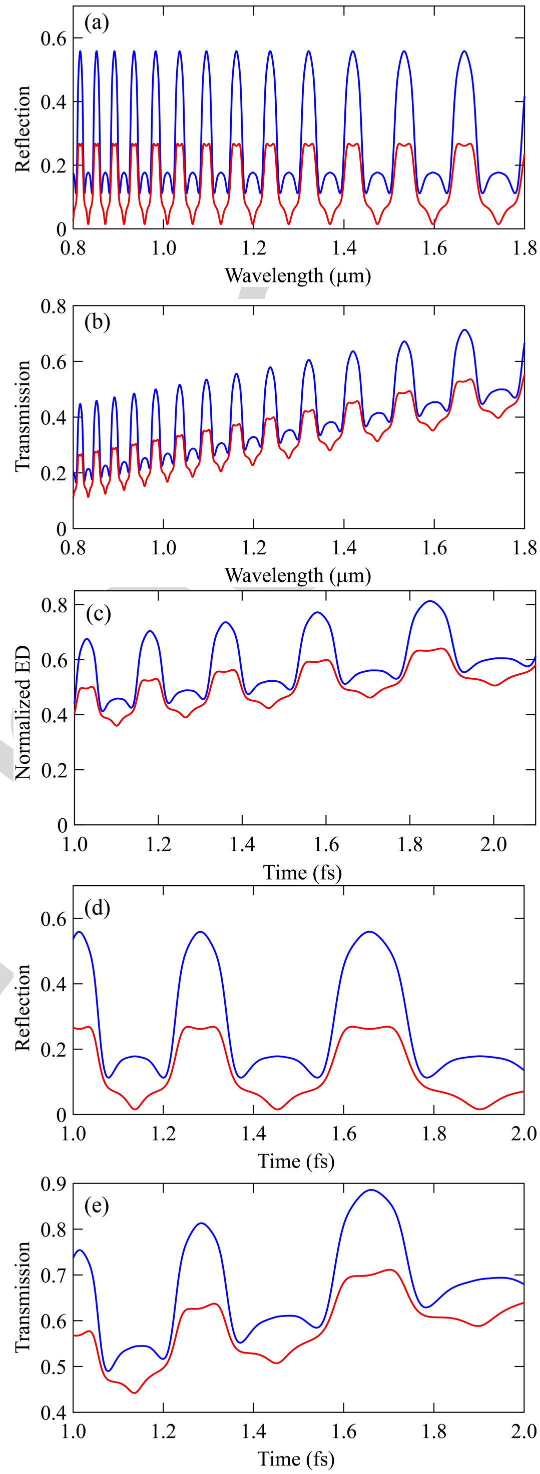

Fig. 7. (a-b) the plot of the normalized reflection and transmission spectra, where the optimum FSR of 0.14μ m is obtained, (c-e) the plot of the interference, reflection and transmission spectra in the time domain, where the transmission bits of 10Pbits^{-1}, and 6Pbits^{-1} are obtained, respectively.

introduced by the optical path difference results in the change in the electron cloud density. The plot of the spins and the optical path difference is shown in Figure 8(a). The increase in the amplitude coefficient, transmission coefficient, and interference function increase the number of electron cloud spins of the spectral profile of the microring Fabry-Perot structure.

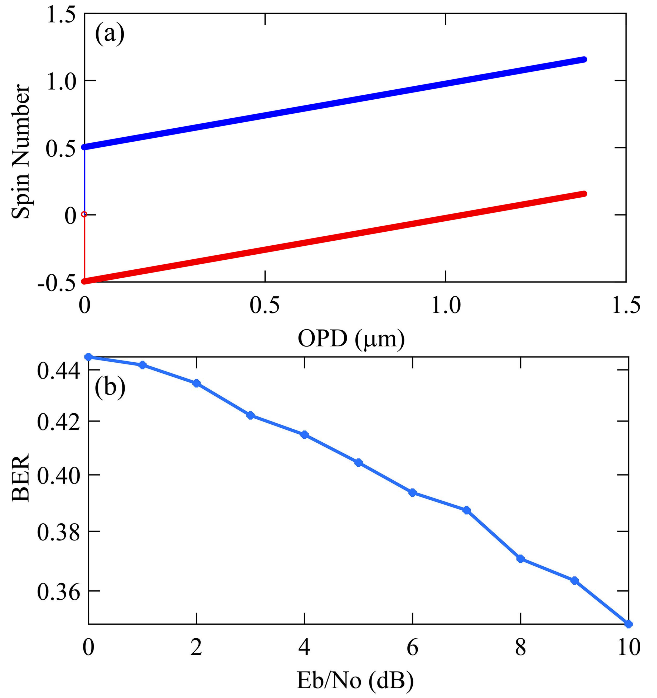

Fig. 8. (a) the plot of spins and OPD, where the sensitivity of 0.2 μm^{-1} is achieved, (b) the BER of 0.35 is obtained, where Eb/No: Energy per bit/noise spectral density.

The schematic structure shown in Figure 1 is configured with realistic parameters and is tested using the AWGN (Additive White Gaussian Noise) communication channel. The calculation of the bit error rate (BER) is employed to validate the simulation. The AWGN communication channel is applied with a 10dB signal to noise ratio. The input signals are modulated, from which the demodulated signals can be retrieved. The BER validates the operational performance of the circuit. The lower the BER, the better the operational performance of the circuit. From Figure 8(b), the BER value of 0.35 is obtained.

IV. Conclusion

A microring Fabry-Perot structure is proposed for the sensing and measurement of electron cloud spins. The gold plate at the center ring induces the polariton that forms the plasmonic wave oscillations. The light excites the gold plate leading to electron cloud oscillations that forms the electron density resulting in the spin-up and spin-down switching. The electron cloud spins transmitted by spin waves and the spectral profile of these spins can be observed in a large bandwidth. In manipulation, the gap between the two Bragg gratings is varied from 200-1000nm with the change in optical path difference where the free spectral range is obtained. The interference spectra of the electron cloud with a varied Bragg grating gap of 200-1000nm have been obtained. By using the given space-time control, the optimum reflection and transmission free spectral range are $\sim$0.14μm. Both the reflection and transmission spectra of the microring Fabry-Perot sensors with a varied Bragg grating gap of 200-1000nm are $\sim$6Pbits^{-1} in terms of quantum bits, while for the interference spectrum has $\sim$10Pbit s^{-1}. The microring Fabry-Perot sensors has a sensitivity of $0.31(\mu m)^{-1}$, however, the sensitivity can be changed by changing the space-time control function. In application, the microring Fabry-Perot sensor can be used for quantum spectroscopy, and quantum sensor, especially for a microscopic regime, where the interference fringes of the spin-waves can be related to the optical path difference and interpreted.

Acknowledgment

The authors would like to acknowledge the research facilities from Ton Duc Thang University, Vietnam.

References

[1] E. Bozo *et al.*, "Cu-Pd bimetal and CuPt alloy nanotubes derived from cu nanowires: Novel amplification media for surface-enhanced Raman spectroscopy," *IEEE Sensors J.*, vol. 20, no. 1, pp. 143–148, Jan. 2020.
[2] F. Li, M. Du, and L. Xu, "Study of dynamic behaviors of thermoacoustic oscillations by using laser absorption spectroscopy," *IEEE Sensors J.*, vol. 19, no. 24, pp. 12271–12278, Dec. 2019.
[3] I. J. Kim and I. Yun, "Real-time plasma uniformity measurement technique using optical emission spectroscopy with revolving module," *IEEE Sensors J.*, vol. 19, no. 6, pp. 2356–2361, Mar. 2019.
[4] N. Z. Gurel, H. Jung, S. Hersek, and O. T. Inan, "Fusing near-infrared spectroscopy with wearable hemodynamic measurements improves classification of mental stress," *IEEE Sensors J.*, vol. 19, no. 19, pp. 8522–8531, Oct. 2019.
[5] J. Sun *et al.*, "Tuning efficiency of distributed feedback laser diode for wavelength modulation spectroscopy," *IEEE Sensors J.*, vol. 19, no. 21, pp. 9722–9727, Nov. 2019.
[6] B. Kashyap, C. K. Sestok, A. G. Dabak, S. Ramaswamy, and R. Kumar, "Ultra-precision liquid level sensing using impedance spectroscopy and data analytics," *IEEE Sensors J.*, vol. 19, no. 20, pp. 9468–9478, Oct. 2019.
[7] G. Giudice, A. Sciuto, A. Meli, G. D'Arrigo, and D. Longo, "SO_2monitoring with solid state-based UV spectroscopy compact apparatus," *IEEE Sensors J.*, vol. 19, no. 16, pp. 7089–7094, Aug. 2019.
[8] S. Gomri *et al.*, "A noise spectroscopy-based features extraction method to detect two gases using one single MOX sensor," *IEEE Sensors J.*, vol. 19, no. 20, pp. 9063–9070, Oct. 2019.
[9] L. Zhang, H. Ding, L. Lin, Y. Wang, X. Guo, and H. Tian, "Transmission versus reflection spectroscopy for discrimination of human and nonhuman blood," *Infr. Phys. Technol.*, vol. 99, pp. 1–4, Jun. 2019.
[10] S. Zvánovec *et al.*, "The use of the Fabry–Pérot interferometer for high resolution microwave spectroscopy," *J. Mol. Spectrosc.*, vol. 256, pp. 141–145, Jul. 2009.
[11] L. Ding, J. Li, Y. Deng, S. Xiao, J. Wang, and Y. Tian, "An inline fiber curvature sensor based on eccentric core fiber and off-axis air cavity Fabry–Pérot interferometer," *IEEE Sensors J.*, vol. 19, no. 19, pp. 8700–8705, Oct. 2019.
[12] I. Yulianti, A. S. M. Supa'at, S. M. Idrus, and M. R. S. Anwar, "Design of fiber Bragg grating-based Fabry–Pérot sensor for simultaneous measurement of humidity and temperature," *Optik*, vol. 124, no. 19, pp. 3919–3923, Oct. 2013.
[13] A. Pospori and D. J. Webb, "Stress sensitivity analysis of optical fiber Bragg grating-based Fabry–Pérot interferometric sensors," *J. Lightw. Technol.*, vol. 35, no. 13, pp. 2654–2659, Jul. 1, 2017.
[14] Q. Wang, M.-B. Liu, P. Wang, and Y. Zhao, "Determination of concentration and temperature by a Fabry–Pérot cavity formed by two fiber Bragg gratings," *Instrum. Sci. Technol.*, vol. 42, no. 4, pp. 412–422, Jul. 2014.
[15] D. Tosi, "Advanced interrogation of fiber-optic Bragg grating and Fabry–Pérot sensors with KLT analysis," *Sensors*, vol. 15, no. 11, pp. 27470–27492, 2015.
[16] A. Wada, S. Tanaka, and N. Takahashi, "Multi-point strain measurement using Fabry–Pérot interferometer consisting of low-reflective fiber Bragg grating," *Jpn. J. Appl. Phys.*, vol. 56, no. 11, pp. 112502-1–112502-6, Nov. 2017.
[17] A. Madan, S. H. K. Yap, V. Paulose, W. Chang, P. P. Shum, and J. Hao, "Investigation of a Bragg grating-based Fabry–Pérot structure inscribed using femtosecond laser micromachining in an adiabatic fiber taper," *Appl. Sci.*, vol. 10, no. 3, p. 1069, 2020.

[18] M. F. Domingues *et al.*, "Cost-effective optical fiber pressure sensor based on intrinsic Fabry–Pérot interferometric micro-cavities," *Opt. Fiber Technol.*, vol. 42, pp. 56–62, May 2018.

[19] N. Pornsuwancharoen *et al.*, "Micro-current source generated by a WGM of light within a stacked silicon-graphene-Au waveguide," *IEEE Photon. Technol. Lett.*, vol. 29, no. 21, pp. 1768–1771, Nov. 1, 2017.

[20] K. Chaiwong, M. Bahadoran, I. S. Amiri, P. Youplao, N. Pornsuwancharoen, and P. Yupapin, "Electro-optic conversion circuit incorporating a fiber optic loop for light fidelity up-down link use," *Microw. Opt. Technol. Lett.*, vol. 61, no. 2, pp. 526–531, Feb. 2019.

[21] M. Bunruangses *et al.*, "Microring distributed sensors using space-time function control," *IEEE Sensors J.*, vol. 20, no. 2, pp. 799–805, Jan. 2020.

[22] S. Tunsiri, N. Thammawongsa, T. Threepak, S. Mitatha, and P. Yupapin, "Microring switching control using plasmonic ring resonator circuits for super-channel use," *Plasmonics*, vol. 14, no. 6, pp. 1669–1677, Dec. 2019.

[23] A. E. Arumona, I. S. Amiri, and P. Yupapin, "Plasmonic micro-antenna characteristics using gold grating embedded in a panda-ring circuit," *Plasmonics*, vol. 15, no. 1, pp. 279–285, Feb. 2020.

[24] P. Phatharacorn, S. Chiangga, and P. Yupapin, "Analytical and simulation results of a triple micro whispering gallery mode probe system for a 3D blood flow rate sensor," *Appl. Opt.*, vol. 55, no. 33, pp. 9504–9513, Nov. 2016.

[25] Photonics Simulation Software. *OptiFDTD Technical Background and Tutorials (Finite Difference Time Domain), Version 12.0*. Accessed: Sep. 20, 2019. [Online]. Available: http://www.optiwave.com

[26] A. M. Prabhu, A. Tsay, Z. Han, and V. Van, "Extreme miniaturization of silicon add–drop microring filters for VLSI photonics applications," *IEEE Photon. J.*, vol. 2, no. 3, pp. 436–444, Jun. 2010.

[27] K. Wiesner, "Quantum cellular automata," in *Encyclopedia of Complexity and Systems Science*, R. Meyers, Eds. New York, NY, USA: Springer, 2009.

A. E. Arumona is currently pursuing the joint Ph.D. degree with the Computational Optics Research Group, Advanced Institute of Materials Science, Ton Duc Thang University, Ho Chi Minh City, Vietnam, the Faculty of Applied Sciences, Ton Duc Thang University, and the Division of Computational Physics, Institute for Computational Science, Ton Duc Thang University. His current research interests are plasmonic electronics, relativistic electronics, and quantum electronics.

Anita Garhwal is currently pursuing the Ph.D. degree with the Amity School of Engineering and Technology (ASET), Amity University Rajasthan (AUR), Jaipur, India. She is a Ph.D. Intern Student with the Advance Institute of Material Science, Ton Duc Thang University, Ho Chi Minh City, Vietnam. Her research interests include micro strip patch antenna, fractal antenna, spin waves, and quantum communication.

Phichai Youplao received the B.Eng. degree in electrical engineering from North Eastern University, Khon Kaen, in 1998, the M.Eng. degree in electrical engineering from Mahanakorn University of Technology, Bangkok, Thailand, in 2005, and the D.Eng. degree in electrical engineering from the King Mongkut's Institute of Technology Ladkrabang, Bangkok, in 2013. He is an Assistant Professor with the Department of Electrical Engineering, Faculty of Industry and Technology, Rajamangala University of Technology Isan Sakon Nakhon Campus, Sakon Nakhon, Thailand, and a Researcher Member with the Computational Optics Research Group, Advanced Institute of Materials Science; Faculty of Applied Sciences, Ton Duc Thang University, Ho Chi Minh City, Vietnam. His current researches of interest are nano-devices and circuits, microring resonator, and quantum cryptography.

Iraj Sadegh Amiri received the B.Sc. degree in applied physics from the Public University of Oroumiyeh, Iran, in 2001, the M.Sc. degree in physics/optics from University Technology Malaysia (UTM) in 2009, and the Ph.D. degree in physics (photonics) in January 2014. He has been performing research on several topics, such as optical soliton communications, laser physics, plasmonics photonics devices, nonlinear fiber optics, optoelectronics devices using 2D materials, waveguides, quantum cryptography, and nanotechnology. He has received the gold medal for his M.Sc. degree.

Kanad Ray (Senior Member, IEEE) received the M.Sc. degree in physics from Calcutta University and the Ph.D. degree in physics from Jadavpur University, West Bengal, India. He has been a Professor of Physics and Electronics and Communication, and is currently working as the Head of the Department of Physics, Amity School of Applied Sciences, Amity University Rajasthan (AUR), Jaipur, India. His current research areas of interest include cognition, communication, electromagnetic field theory, antenna and wave propagation, microwave, computational biology, and applied physics. He has been serving as an Editor for various Springer book series. He was an Associate Editor of the *Journal of Integrative Neuroscience* (The Netherlands: IOS Press).

S. Punthawanunt received the B.Sc. and M.Sc. degrees in computer science from Assumption University, Bangkok, Thailand. He is currently the Dean of the Faculty of Science, Kasem Bundit University, Bangkok. His studies of interest are 5G technologies, multimedia communications, and LiFi networking.

Preecha Yupapin received the Ph.D. degree in electrical engineering from the City, University of London, U.K., in 1993. He is currently the Full Professor with the Computational Optics Research Group, Advanced Institute of Materials Science and a member of the Faculty of Applied Sciences, Ton Duc Thang University, Ho Chi Minh City, Vietnam. His current research interests are nano-devices and circuits, microring resonator, soliton communication, optical motor, quantum technologies, and meditation science.